Journal of Materials Chemistry C

Molecular engineering of π-extended pyrrolo[1,2-a]quinoxaline-based D-A materials for electrochromic devices

Journal:	*Journal of Materials Chemistry C*
Manuscript ID	TC-ART-03-2025-001087.R1
Article Type:	Paper
Date Submitted by the Author:	17-Apr-2025
Complete List of Authors:	Zhao, Kexin; Shaanxi University of Technology Liu, Quan; Shaanxi University of Technology, Chemical and Environmental Science Wang, Wenquan; Shaanxi University of Technology Kang, Chengyi; Shaanxi University of Technology Zhang, Ziyi; Shaanxi University of Technology Xu, Haitao; Shaanxi University of Technology, School of Chemical and Environmental Science Dai, Huiping; Shaanxi University of Technology

ARTICLE

Molecular engineering of π-extended pyrrolo[1,2-α]quinoxaline-based D-A materials for electrochromic devices

Received 00th January 20xx,
Accepted 00th January 20xx

DOI: 10.1039/x0xx00000x

Kexin Zhao [a,b], Wenquan Wang [a,b], Chengyi Kang [a,b], Ziyi Zhang [a,b], Haitao Xu [a,b], Quan Liu [*a,b], Huiping Dai [*c]

Pyrrolo[1,2-α]quinoxaline, a new class of nitrogen-containing skeletons, holds a wide range of applications in the development of optoelectronic materials. In this study, a class of electroactive materials, namely **CH_3-PQ-TPA**, **PQ-TPA** and **CF_3-PQ-TPA**, was constructed by combining triphenylamine with pyrrolo[1,2-α]quinoxaline containing different types of substituents based on a molecular engineering strategy. Calculations and experimental investigations have shown that with the enhancement of electron-withdrawing ability of substituent, the energy gap of the compounds decreases. As a result, CF_3-PQ-TPA exhibits more excellent electrochemical activity. Meanwhile, these materials were further used to fabricate electrochromic devices, in which **CF_3-PQ-TPA**-based devices showed excellent stability and reversibility. This study will provide new molecular design ideas and molecular skeletons for electrochromic materials.

Introduction

Electrochromic materials, which exhibit reversible colour changes when subjected to an external electric stimulus [1-3], have been widely applied in electronic paper [4], electronic shelf label [5], energy storage [6], smart windows [7] and displays [8]. Therefore, these materials have attracted considerable research interest. Among them, organic small molecule electrochromic materials have gained rapid development and research due to their strong designability of molecular structure and high optical contrast [9,10]. Triphenylamine (TPA) moiety is a nitrogen-containing organic small molecule composed of three aromatic groups. It has been proven to possess unique photoelectric properties, such as excellent redox activity, high carrier transport capability, and strong thermal stability [11-13]. In addition, triphenylamine can be easily oxidized into stable radical cations, resulting in changes in appearance colour [14]. Therefore, triphenylamine-based compounds hold significant potential for the construction and development of stimulus-responsive materials [15-18].

Donor-acceptor (D-A) structure is one of the important strategies in the design of electrochromic materials. The chromic properties of the molecules can be finely tuned by changing the substituents or adjusting the conjugated system [19,20]. Recently, Mo et al. connected the donor (TPA) and acceptor (EDOT) units via π-conjugated bridges to enhance the conjugation effect between the segments, thereby improving the overall charge transport capability of the molecules. They introduced different electron-donating substituents (-Ph, -OCH_3) at the para position of the TPA unit to modulate the initial oxidation potential, optical bandgap, and electrochromic properties of the molecules [21].

Skene and co-worker modified the electron-accepting ability of benzothiadiazole derivatives using varying electron-withdrawing groups (-H, -CHO, -CN, -NO_2). Combined with the donor TPA unit, four donor-acceptor materials were created [22]. The study found that increasing the electron acceptor strength effectively modulated the emission characteristics, causing a red shift in emission wavelength. This is due to the increased charge transfer in the material's excited state. Moreover, materials with stronger electron-withdrawing groups (-NO_2) exhibited the highest absorption intensity from electrochemical oxidation. In contrast, materials with weaker electron-withdrawing groups (-CHO) showed 4% lower absorption than -NO_2-substituted materials. The absorption of acceptors with -H groups was lower than that of acceptors with electron-withdrawing groups. Therefore, enhancing acceptor strength with electron-withdrawing groups aids in developing high-contrast electrochromic materials.

[a.] *Shaanxi Province Key Laboratory of Catalytic, Shaanxi University of Technology, Hanzhong 723001, P. R. China.*
[b.] *School of Chemical and Environmental Science, Shaanxi University of Technology, Hanzhong 723001, P. R. China.*
[c.] *School of Biolegical Science and Engineering, Shaanxi University of Technology, Hanzhong 723001, P. R. China.*
Electronic Supplementary Information (ESI) available: [details of any supplementary information available should be included here]. See DOI: 10.1039/x0xx00000x

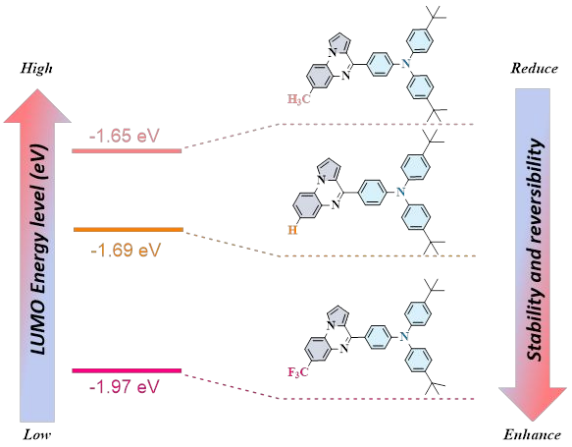

Fig. 1 Structure and material design of pyrrolo[1,2-α]quinoxaline derivatives **CH_3-PQ-TPA**, **PQ-TPA**, and **CF_3-PQ-TPA**.

Pyrrolo[1,2-α]quinoxaline (PQ) derivatives are important polycyclic compounds with highly conjugated, rigid, planar structures and excellent photoelectric properties [23]. Their structural modifiability allows for the adjustment of photophysical properties through different functional groups, facilitating the development of various photoelectric materials, such as chemical sensors [24] and electroluminescent devices [25]. Based on these considerations, in this paper, TPA derivatives and PQ are combined to create photoelectric functional molecules with donor-acceptor (D-A) structures. Introducing -CH_3 and -CF_3 substituents on the PQ regulates the acceptor strength, investigating the impact of different acceptor strengths on molecular properties (**Fig.1**). Consequently, three novel electroactive materials **CH_3-PQ-TPA**, **PQ-TPA**, and **CF_3-PQ-TPA** were designed and synthesis. By studying their photophysical and electrochemical properties, along with theoretical calculations, the effects on the photoluminescence (PL) characteristics and electrochromic (EC) of devices made from these materials were systematically explored. This research provides a reference for the further development of pyrrolo[1,2-α]quinoxaline-based photoelectric active materials.

Experimental section

Materials and reagents

All chemicals and reagents were purchased from commercial sources and used as received. 4-bromobenzaldehyde, 4,4'-di-tert-butyldiphenylamine, tris(dibenzylideneacetone)dipalladium(0), were purchased from Energy Chemical. Ferrocene (Fc), XPhos, anhydrous sodium sulfate and cesium carbonate were purchased from J&K Chemical Ltd. All other reagents, including Toluene, ethanol, and acetic acid were purchased from Sinopharm Chemical Reagent Co. Ltd. Indium tin oxide (ITO) glass (< 17 Ω/sq) was used after cleaning ultrasonically in deionized water, ethanol, acetone, and deionized water, successively.

Measurements and characterization

With tetramethylsilane (TMS) as the internal standard, ^{1}H NMR spectra and ^{13}C NMR spectra were recorded on a Bruker A 400 spectrometer at 400 MHz and 100 MHz in Chloroform-*d* solvent. High resolution mass spectrometry (HRMS) data were measured by SCIEX X500R QTOF instrument. UV-Vis absorption spectra were measured by Shimadzu UV-3900 spectrophotometer. Fluorescence measurements were performed on a Hitachi F-4600 spectrophotometer. Fluorescence lifetimes were measured at room temperature and in air using an Edinburgh FLS1000 instrument. Thermo gravimetric analysis (TGA) was performed on NETZSCH STA 499 F5 at temperatures ranging from room temperature to 800 °C with a heating rate of 10 °C/min. Single-crystal X-ray diffraction was carried out at room temperature using MoK_α or CuK_α on a BRUKERD8QUEST diffractometer. Cyclic voltammetry curves were performed at electrochemical workstation CHI600D. A three-electrode cell was constructed with Pt wire electrode as the working electrode, Pt wire as the counter electrode, and Ag/Ag^+ electrode as the reference electrode. The scan rate was 100 mV/s. The solution for electrochemical studies was prepared by dissolving $TBAPF_6$ in DCM/ACN (1:1, V/V) solvent.

DFT calculations

All the structures involved in this paper were calculated using the Gaussian 09 software package. The geometric structures of the compounds were optimized using the density functional method, with the B3LYP functional and 6-31G (d,p) basis set. Global optimization and frequency calculations were performed for all structures. The spin density distributions (SDDs) of structures were obtained in UB3LYP/6-31G (d,p) level, All structures properties were analyzed using the Multiwfn 3.8 software, and visualization was carried out using the VMD software.

Fabrication of EC devices

The procedure for preparing electrochromic devices are as follows. The ITO conductive glass (2 cm × 4 cm × 1.1 mm, < 17 Ω/sq) need to be pretreated, followed by ultrasonic cleaning with deionized water, ethanol, acetone and deionized water, respectively. After drying under nitrogen atmosphere for solvent removal, two pieces of ITO-coated glass were adhesived face-to-face with 3 M double-sided adhesive tape (width: 4 mm, thickness: 0.5 mm) and form a cavity between them. The active area of each device was around 1.0 cm × 2.5 cm. This small cavity for later injection of the corresponding electrochromic active solution containing 1 × 10^{-3} M π-extended pyrrolo[1,2-α]quinoxaline derivatives (**CH_3-PQ-TPA**, **PQ-TPA**, and **CF_3-PQ-TPA**) and 0.1 M $TBABF_6$ in DCM/ACN (1:1, V/V), which was eventually sealed completely with UV gel. (**Fig. 2**)

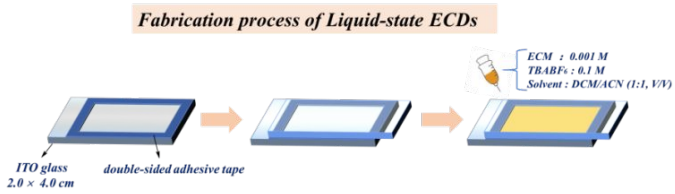

Fig. 2 Fabrication process of liquid-state EC devices.

Results and Discussion

Synthesis and characterization

As shown in **Scheme 1**, Compound **3** synthesized via electrophilic cyclization reaction was synthesized with 4,4′-di-*t*-BuDPA via Buchwald-Hartwig coupling reaction catalyzed by a palladium catalyst to synthesize the final product [26-29]. The detailed synthesis steps are described in the Supporting Information. The ^{1}H NMR, ^{13}C NMR and HRMS spectra of the intermediate and final products are displayed in Supporting Information.

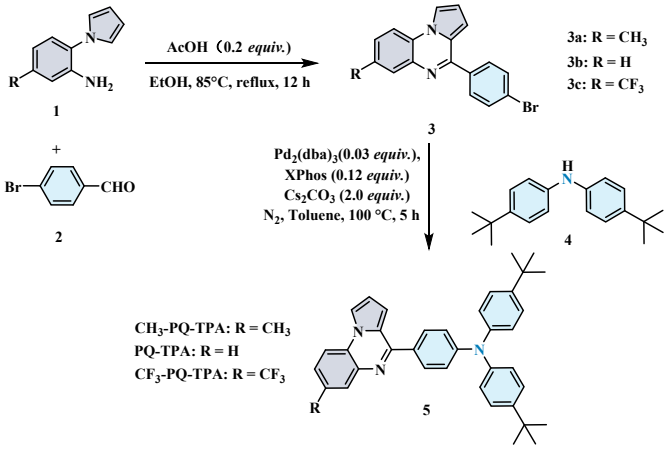

Scheme 1. Synthesis routes of π-extended pyrrolo[1,2-*α*]quinoxaline derivatives **CH_3-PQ-TPA**, **PQ-TPA** and **CF_3-PQ-TPA**.

Photophysical properties and thermal stability

The ultraviolet-visible absorption and photoluminescence spectra of compounds **CH_3-PQ-TPA**, **PQ-TPA** and **CF_3-PQ-TPA** are depicted in **Fig. 3a**, with maximum absorption wavelengths at 377 nm, 376 nm, and 388 nm, respectively, which are attributed to the absorption resulting from π-π* transitions [30]. The maximum emission wavelengths of **CH_3-PQ-TPA**, **PQ-TPA** and **CF_3-PQ-TPA** are 517 nm, 521 nm, and 532 nm, respectively, which are attributed to the emission resulting from molecular charge transfer [31]. Due to the enhanced electron-accepting ability of the acceptor PQ (CH_3 < H < CF_3), the intramolecular charge transfer effect gradually increases, hence, **CF_3-PQ-TPA** exhibits the longest emission wavelength. The emission spectra of the three compounds in solvents of different polarities are shown in **Fig. 3d-f**, respectively. With the increase of solvent polarity, the three compounds showed obvious solvatochromism, which further indicated that the emission peaks of these three compounds originate from intramolecular charge transfer. The Lippert-Mataga models are displayed in **Fig. 3g-h**, respectively, with the excited-state dipole moments of the three compounds being 11.91 D, 12.33 D, and 16.39 D (**Table S1-S3**) [32-34]. Building on these findings, we further explored the material's fluorescence attenuation behavior under $Cu(ClO_4)_2$ titration, as shown in **Fig. S13**. Combined with the solvent-dependent fluorescence data, this behavior highlights its potential for electrofluorochromic applications, where external electric fields could dynamically control emission properties. **Fig. 3b** illustrates that the fluorescence lifetimes of the three compounds are 4.68 ns, 4.36 ns, and 5.62 ns, respectively; As demonstrated in **Fig. 3c**, all three compounds exhibit good stability, with thermal decomposition temperatures of 358 °C, 298 °C, and 317 °C, respectively.

Electrochemical properties

As shown in **Fig. 4a-c**, the CV curve exhibited two pairs of redox peaks centered at neutral state or radical cation state transition in the nitrogen atom of triphenylamine segments in the potential range of 0 V ~ 1.8 V (*vs*. Ag/Ag$^+$) [35,36]. The effects of the substituent on the pyrrolo[1,2-*α*]quinoxaline core on the oxidation potential were examined and the data were gathered in **Table 1.** As we expected, the substituent on the pyrrolo[1,2-*α*]quinoxaline core with electro-donating substituents like methyl (**CH_3-PQ-TPA**) is more easily oxidized than those with electro-withdrawing substituents like trifluoromethyl group (**CF_3-PQ-TPA**) [37,38]. In fact, the oxidation potential value of electro-donating group leads to much lower than that of electro-withdrawing group. We concluded that the apparent reversible redox peaks at 1.10 V, 1.11 V and 1.19 V of the compounds **CH_3-PQ-TPA**, **PQ-TPA** and **CF_3-PQ-TPA** were attributed to the formation of cationic radicals by single-electron oxidation of the nitrogen atomic center of triphenylamine, while the anode peaks at 0.9 V were attributed to the oxidation of $TBAPF_6$ [39,40]. Among three compounds, **CH_3-PQ-TPA** has the lowest first oxidation peak at 1.10 V, indicating that the electron-giving ability and IV-CT resonance effect between TPA center and methyl group are the strongest. With the increase of applied potential, the second oxidation peak of **CH_3-PQ-TPA** appeared at 1.27 V, indicating that the pyrrolo[1,2-*α*]quinoxaline structure produced additional redox active sites as shown in **Scheme 2** and **Fig. S14** [41,42]. The other compounds showed similar CV curves to that of **CH_3-PQ-TPA** with second oxidation peak at 1.28 V (**PQ-TPA**) and 1.37 V (**CF_3-PQ-TPA**). The redox capacity and electrochromic reversibility of **CF_3-PQ-TPA** remained almost constant during repeated scanning between 0 and 1.8 V. This result confirms that the substitution of -CF_3 groups on the acceptor gives the cationic radical and dication state considerable stability. This is because the electronic effects of substituents, such as electro-withdrawing or electro-donating effects, can significantly affect the electrochemical stability of molecules. Electro-withdrawing groups can reduce the

electron cloud density of molecules, thereby reducing the interaction between molecules and electrolytes and improving electrochemical stability. Electro-donating groups can increase the electron cloud density of molecules, which may enhance their reactivity, but may also make them more susceptible to oxidation or reduction, thereby affecting stability [43].

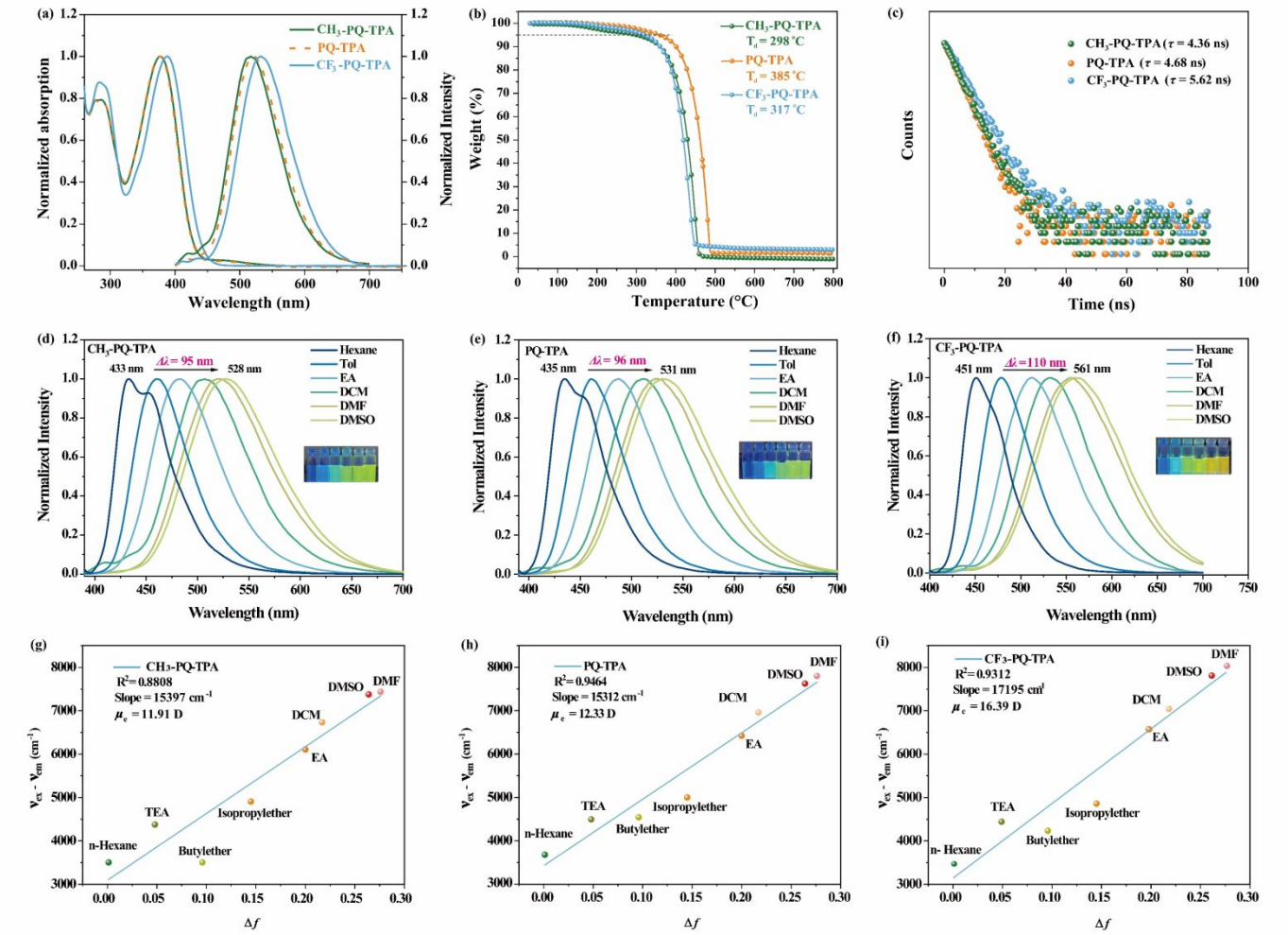

Fig. 3 (a) Ultraviolet-visible (UV-vis) absorption and photoluminescence spectra of compounds **CH_3-PQ-TPA**, **PQ-TPA** and **CF_3-PQ-TPA** in the DCM (1×10-5 M). (b) Fluorescence lifetime in solution. (c) Thermo gravimetric analysis. (d) Photoluminescence spectra of **CH_3-PQ-TPA** and (e) **PQ-TPA** and (f) **CF_3-PQ-TPA** in different polar solvents. (g) Lippert-Mataga model of **CH_3-PQ-TPA** and (h) **PQ-TPA** and (i) **CF_3-PQ-TPA.**

Table 1. Thermal, electrochemical properties and photophysical data of **CH_3-PQ-TPA**, **PQ-TPA** and **CF_3-PQ-TPA**.

	Experimental							Calculated		
Compound	E_{ox} (V)	E_{red} (V)	E_{HOMO} (eV)[a]	E_{LUMO} (eV)	E_g (Ev)[b]	T_d(°C)	τ/ns	E_{HOMO} (eV)	E_{LUMO} (eV)	E_g (eV)
CH_3-PQ-TPA	1.10/1.27	1.02/1.20	-5.14	-2.21	2.93	259	4.36	-5.05	-1.65	3.40
PQ-TPA	1.11/1.28	1.04/1.21	-5.14	-2.22	2.92	358	4.68	-5.08	-1.69	3.39
CF_3-PQ-TPA	1.19/1.37	1.12/1.30	-5.26	-2.44	2.82	317	5.62	-5.20	-1.97	3.23

[a] The HOMO energy levels were calculated from cyclic voltammetry and were referenced to ferrocene (4.8 eV).

[b] The data were calculated from compounds by the equation E_g =1240/λ_{onset}.

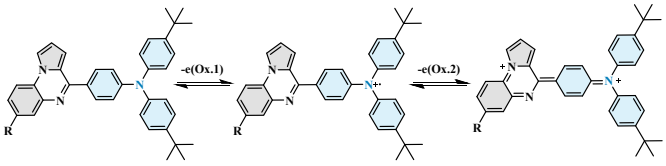

Scheme 2. Redox process of π-extended pyrrolo[1,2-*α*]quinoxaline derivatives.

The electron transfer constant of the molecule during the redox process can be calculated from the measured cyclic voltammetry curve according to the Nicholson method. Setting different sweep speeds from 20 mV•s^{-1} to 1000 mV•s^{-1} to test the CV curves of compounds **CH_3-PQ-TPA**, **PQ-TPA** and **CF_3-PQ-TPA** as shown in **Fig. S15**. The ip~$v^{1/2}$ curve was obtained by plotting

according to the Randles-Sevcik equation, and the slope R was calculated from the curve. **CH_3-PQ-TPA**: $R_1 = 4.20 \times 10^{-5}$, $R_2 = 5.90 \times 10^{-5}$; **PQ-TPA**: $R_1 = 3.57 \times 10^{-5}$, $R_2 = 5.81 \times 10^{-5}$; **$CF_3$-PQ-TPA**: $R_1 = 4.95 \times 10^{-5}$, $R_2 = 3.65 \times 10^{-5}$. When the scanning rate is set to 100 mV • s^{-1}, the electron transfer constant in the one-electron redox process of **CH_3-PQ-TPA**, **PQ-TPA** and **CF_3-PQ-TPA** can be calculated according to the Nicholson formula. **CH_3-PQ-TPA**: $k_{ET1} = 1.3 \times 10^{-3}$, $k_{ET2} = 1.4 \times 10^{-3}$; **PQ-TPA**: $k_{ET1} = 1.6 \times 10^{-3}$, $k_{ET2} = 2.3 \times 10^{-3}$; **$CF_3$-PQ-TPA**: $k_{ET1} = 1.5 \times 10^{-3}$, $k_{ET2} = 1.7 \times 10^{-3}$ [8] (Table S4).

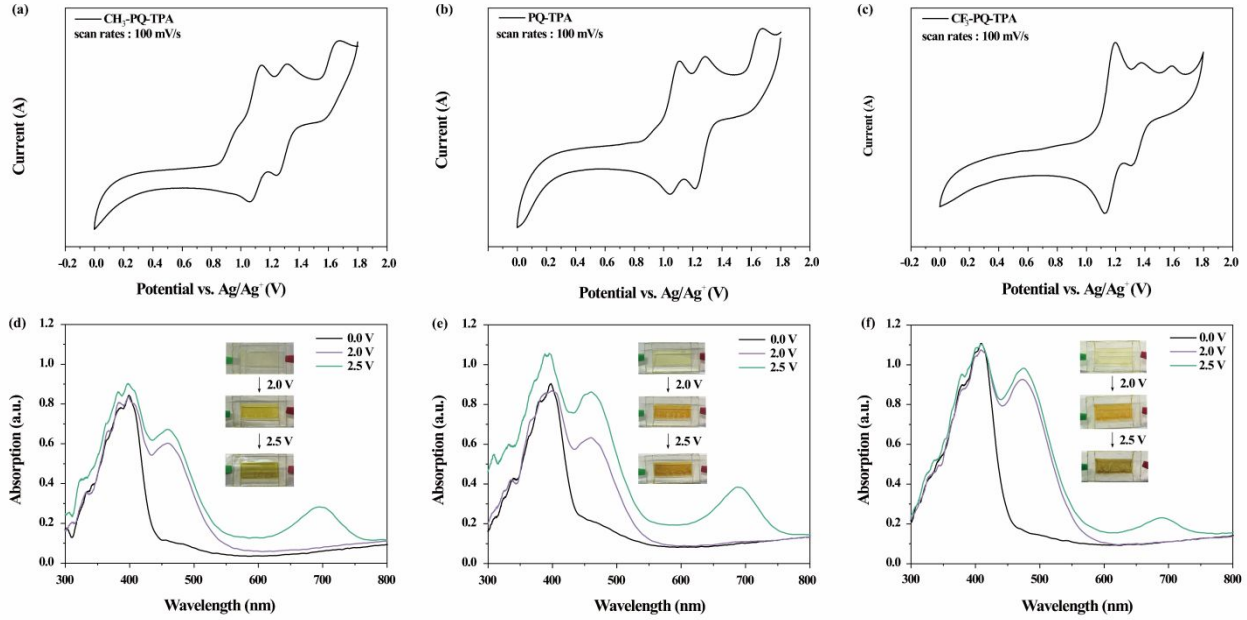

Fig. 4 (a) Cyclic voltammetry of compound **CH_3-PQ-TPA** and (b) **PQ-TPA** and (c) **CF_3-PQ-TPA** (1×10^{-3} M) in DCM/ACN (1:1, V/V) solvent and 0.1 M Bu_4NPF_6 are referenced to the Ag/Ag^+ couple. Scan rate: 100 mV•s^{-1}. (d) Spectral change of the electrochemical device of **CH_3-PQ-TPA** and (e) **PQ-TPA** and (f) **CF_3-PQ-TPA**. The inset shows the photographic images of the electrochemical device at indicated applied voltages.

Electrochromic properties

Following the electrochemical tests, the optical properties of the electrochromic device (ECD) were evaluated by using spectroelectrochemistry. **Fig. 4d-f** shows absorption-wavelength-applied potential correlations of this sample. In the neutral form, at 0 V, the compound **CH_3-PQ-TPA** exhibits strong absorption at wavelength 378 nm, characteristic for triphenylamine, which supports our assumption of the $TPA^{\bullet+}$ formation, but it was almost transparent in the visible region. The absorption peaks of **PQ-TPA** and **CF_3-PQ-TPA** in the initial neutral state are at 377 nm and 388 nm. With increasing applied voltage from 0 to 2.0 V, the intensity of the absorption peak at 460 nm gradually increased. In addition, **PQ-TPA** and **CF_3-PQ-TPA** showed similar EC properties, and their color-changing wavelengths are 462 nm and 475 nm, respectively. We attributed this spectral change to the formation of stabilizing cationic radicals in the TPA structure within the compounds. As the applied voltage was increased to 2.5 V, a new broadband was formed centered at 695 nm. This spectral change could be attributable to the formation of a dictation [41]. The UV-visible absorption changes observed in ECD at different potentials are fully reversible and are accompanied by strong color changes. Without voltage or with negative voltage the radical cation becomes neutral molecule again. The fully reversible EC mechanism provided feasibility for the fabrication of EC devices. In fact, these changes can even be readily observed with the naked eye. As can be seen in **Fig. 4d-f** inset, the ECD of **CH_3-PQ-TPA** shifted from a transmissive neutral state (light yellow) to a highly absorbing semi-oxidized (yellow) and fully oxidized (brown or orange) state.

The definition of the coloration efficiency (η) describes the change in the optical density of the device when the unit charge is injected or extracted during the color change of the device. The coloration efficiency (η) is an essential factor in deciding the coloring ability for an ECD under a certain amount of charge consumption.

$$\eta = \frac{\Delta OD}{Q} \; ; \Delta OD = \log\frac{T_b}{T_c}$$

Where η is the coloring efficiency (cm^2/C); ΔOD is the change in optical density; Q is the amount of charge injected (or extracted) per unit area (cm^2/C); T_c is the transmittance of the colored state (%); T_b is thetransmittance (%) of the faded state [44]. As shown in **Fig. S18**, the slope of the linear regression of the plot represents the coloring efficiency (η) of ECD, **CF_3-PQ-TPA** has the highest η (655.52 cm^2/C) among the three devices, which means it has the highest ΔOD at the same charge consumption and energy efficiency. **CH_3-PQ-TPA** and **PQ-TPA** exhibit similar coloring efficiencies, with values of 316.38 cm^2/C and 306.58 cm^2/C, respectively.

Chemical oxidation

As mentioned earlier, these triphenylamine derivatives have almost no absorption in the visible region in the neutral state, and furthermore, the generation of the triphenylamine radical cation or cation can be achieved by electrochemical or chemical oxidation [45]. $Cu(ClO_4)_2$ has recently been reported to be a mild and clean oxidizing agent that effectively generates arylamine cation radicals, and most importantly, at low concentrations, it does not absorb or emit in the UV-visible domain [46-48]. The cationic radicals of triphenylamine derivatives generated by $Cu(ClO_4)_2$ in DCM/ACN (1:1, V/V) solvent were characterized by UV absorption spectroscopy. After titration with 1.0 equivalents of $Cu(ClO_4)_2$, the original absorption peak of compound **CH_3-PQ-TPA** at 372 nm decreased and new absorption peaks gradually appeared at 475 nm and 688 nm, compound **PQ-TPA** showed new absorption peaks at 461 nm and 686 nm, and new absorption peaks of compound **CF_3-PQ-TPA** appeared at 476 nm and 689 nm (**Fig. 5**). The longer wavelength peaks all commenced from the addition of 0.6 eq. This is due to the fact that the triphenylamine structure in the compound generate a radical cation under the oxidation of $Cu(ClO_4)_2$, and subsequently a portion of the radical cation undergoes secondary oxidation to the cationic state.

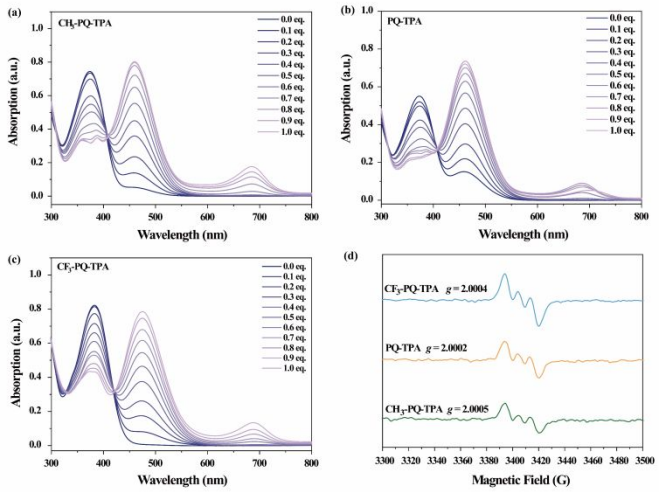

Fig. 5 (a) Absorption spectra recorded upon oxidation of **CH_3-PQ-TPA** and (b) **PQ-TPA** and (c) **CF_3-PQ-TPA** by $Cu(ClO_4)_2$ in DCM/ACN (1:1, V/V) solvent. (d) EPR spectra and *g* factor of the radical species of **CH_3-PQ-TPA**, **PQ-TPA** and **CF_3-PQ-TPA**.

Essentially, in chemical oxidation titration experiments, the formation of new absorption bands in the UV-vis regions suggests the formation of radical cations of the aromatic amines after the electron transfer reaction of aniline with Cu^{2+} [49]. Electron paramagnetic resonance (EPR) spectroscopy was also tested to investigate the characterization of radical species. It's actually the conversion of TPA into a radical cation. **CH_3-PQ-TPA**, **PQ-TPA** and **CF_3-PQ-TPA** were dissolved separately into DCM/ACN (1:1, V/V) solvent at a concentration of 1×10^{-3} M and then $Cu(ClO_4)_2$ was added to oxidize the compounds to the radical cation. **Fig. 5(d)** illustrates a similar three-line EPR spectrum for compounds **CH_3-PQ-TPA**, **PQ-TPA** and **CF_3-PQ-TPA$^{\bullet+}$** in the 3300-3500 G range for these cationic radicals with *g* values of 2.0005 *g*, 2.0002 *g* and 2.0004 *g* [50,51]. In addition, we have calculated the spin density map of compounds **CH_3-PQ-TPA**, **PQ-TPA** and **CF_3-PQ-TPA$^{\bullet+}$** using the B3LYP/6-31G (d,p) method based on density functional theory (DFT). The spin density distribution of compounds **CH_3-PQ-TPA**, **PQ-TPA** and **CF_3-PQ-TPA$^{\bullet+}$** is located not only on the TPA unit but also on the quinoxaline unit and to a lesser extent on the pyrrolo unit, which leads to significant spin-delocalization due to the compound's attachment of different electron-withdrawing substituents or electron-donating substituents. The result reveals that the spin populations on the TPA unit of **CH_3-PQ-TPA**, **PQ-TPA** and **CF_3-PQ-TPA$^{\bullet+}$** are 0.2761, 0.28538 and 0.30591 [52,53] (**Fig. 6**). Among the three compounds, **CF_3-PQ-TPA$^{\bullet+}$** has the highest spin density, which was in agreement with previous work that electrochemical device of **CF_3-PQ-TPA** possess short coloured times and better cyclic stability (**Fig. S19**) [54].

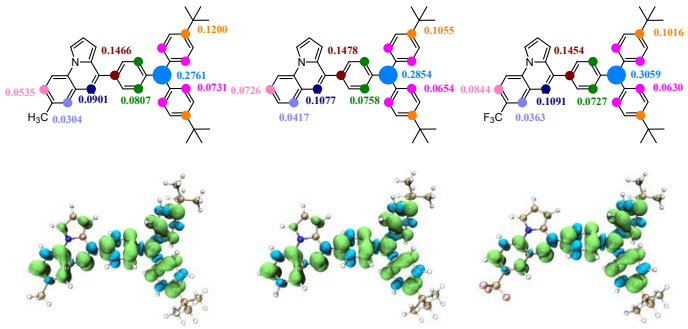

Fig. 6 Mulliken atomic spin density values (up) and spin density map (down) of **CH_3-PQ-TPA**, **PQ-TPA** and **CF_3-PQ-TPA$^{\bullet+}$** at the UB3LYP/6-31G (d, p) level of theory.

Theoretical calculations

In order to investigate the effects of different substituents on the electronic structures of three compounds at the molecular level, we simulated their properties using the B3LYP/6-31G(d,p) method based on DFT [55]. The distribution of the frontier molecular orbitals for compounds **CH_3-PQ-TPA**, **PQ-TPA** and **CF_3-PQ-TPA** are depicted in **Fig. 7**. The highest occupied molecular orbitals (HOMO) are predominantly localized in the diphenylamine and benzene-bridge units, with partial extension into the pyrrolo[1,2-α]quinoxaline unit. Conversely, the lowest unoccupied molecular orbitals (LUMO) are primarily distributed across the pyrrolo[1,2-α]quinoxaline and benzene-bridge units. There is significant overlap between the HOMO and LUMO on the benzene bridge, which ensures that these compounds exhibit strong photoluminescence quantum yields. In terms of HOMO and LUMO, the HOMO indicates the molecule's ability to donate electrons, while the LUMO indicates its ability to accept electrons.

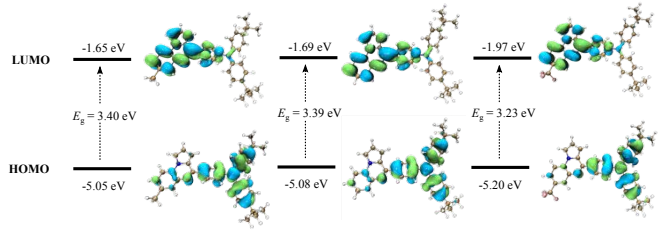

Fig. 7 The HOMO/LUMO orbital distributions and energy level of compounds **CH_3-PQ-TPA**, **PQ-TPA** and **CF_3-PQ-TPA**.

The HOMO and LUMO energy levels of these compounds are -5.05 eV, -5.08 eV, -5.20 eV for HOMO, and -1.65 eV, -1.69 eV, -1.97 eV for LUMO, respectively (**Fig. 7**). The HOMO and LUMO energy levels decrease gradually with the increase in electron-withdrawing ability of the substituent groups. **CF_3-PQ-TPA**, which introduces the electron-withdrawing group -CF_3, exhibits the lowest LUMO energy levels, indicating a higher electron affinity potential, greater oxidizing ability, and a larger reduction potential. Additionally, the energy band gaps (E_g) of the three compounds are 3.40 eV, 3.39 eV, and 3.23 eV, respectively, with **CF_3-PQ-TPA** having the narrowest energy gap. This suggests that **CF_3-PQ-TPA** has the best conductivity. Consequently, **CF_3-PQ-TPA** possesses superior stability and electrochemical properties compared to **CH_3-PQ-TPA** and **PQ-TPA**.

Single-crystal structure analysis

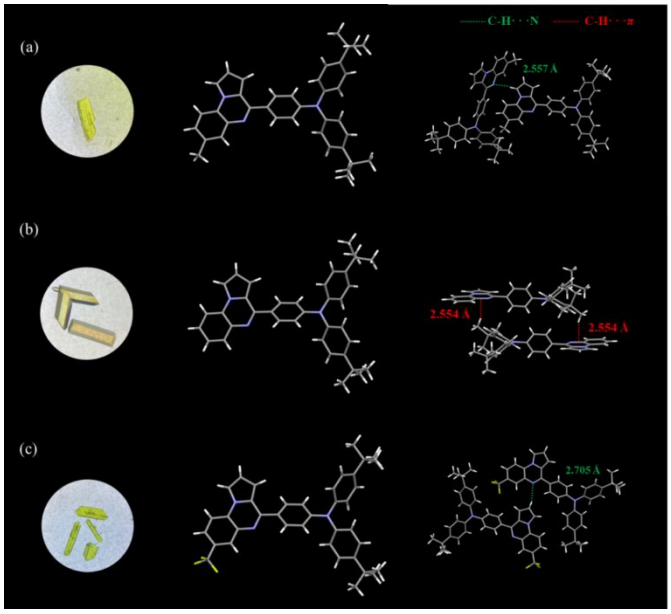

Fig. 8 (a) Single crystal structure, photo and Packing diagram of **CH_3-PQ-TPA** (CCDC: 2270406) and (b) **PQ-TPA** (CCDC: 2400581) (c) **CF_3-PQ-TPA** (CCDC: 2412717).

Single crystals of **CH_3-PQ-TPA** and **PQ-TPA** were then incubated by solution evaporation method between acetonitrile and dichloromethane, and single crystals of **CF_3-PQ-TPA** were incubated in the same way using DMF and dichloromethane and further analyzed by X-ray diffraction to study their molecular packing and intermolecular interactions. As far as the intermolecular level is concerned, it can be noticed that for **PQ-TPA** one hydrogen bond is observed, which is between C-H and π (2.554 Å, marked as red dashed line) (**Fig. 8b** and **Table S6**). Only one hydrogen bond is present in **CH_3-PQ-TPA**, located between C-H and N (2.557 Å, marked with a green dashed line) (**Fig. 8a** and **Table S5**). **CF_3-PQ-TPA** also has a hydrogen bond between C-H and N (2.705 Å, marked with a green dashed line) (**Fig. 8c** and **Table S7**).

Conclusions

In summary, three D-n-A type electroactive materials based on pyrrolo[1,2-*α*]quinoline, namely, **CH_3-PQ-TPA**, **PQ-TPA**, and **CF_3-PQ-TPA**, were designed and synthesized in this study. The substituent effects on photoelectronic properties were systematically investigated through spectral analysis, cyclic voltammetry, and electron paramagnetic resonance spectroscopy. The results demonstrated that the introduction of the strong electron-withdrawing group endowed **CF_3-PQ-TPA** with the lowest LUMO energy level, exhibiting enhanced electron affinity, greater oxidizing capacity, and higher reduction potential. Moreover, **CF_3-PQ-TPA** displays the narrowest band gap 3.23 eV, indicating that it has the best charge transport characteristic among these compounds. Electrochromic testing further revealed that **CF_3-PQ-TPA** maintained exceptional cycling stability and reversibility over 300 consecutive cycles. Therefore, these properties make the pyrrolo[1,2-*α*]quinoline structure promising for applications in the field of electrochromic materials.

Conflicts of interest

There are no conflicts to declare.

Acknowledgements

We acknowledge the Graduate Fund project of Shaanxi University of Technology (SLGYCX2415). We are very grateful to Prof. Jiufu Lu for his assistance in single crystal analysis and Prof. Wei He for her assistance in NMR and HRMS testing.

Notes and references

[1] C. Gu, S. Wang, J. He, Y. M. Zhang and S. X. A. Zhang, *Chem*, 2023 ,**9**, 2841-2854.

[2] B. Lim, S. Y. Han and Y. C. Nah, *Org. Electron.*, 2018, **63**, 23-28.

[3] P. M. Beaujuge and J. R. Reynolds, *Chem. Rev.*, 2010, **110**, 268-320.

[4] A. Fu and M. Serpe., *ACS Appl. Polym. Mater.*, 2022, **4**, 9186-9193.

[5] Y. Wang, S. Wang, X. Wang, W. Zhang, W. Zheng, Y. M. Zhang and S. X. A. Zhang, *Nat. Mater.*, 2019, **18**, 1335-1342.

[6] D. Dalavi, R. Desai and P. Patil, *J. Mater. Chem. A.*, 2022, **10**, 1179-1226.

[7] S. Kandpal, L. Bansal, O. S. Game and R. Kumar, *ACS Appl. Mater. Interfaces*, 2025, **17**, 2703-2715.

[8] R. Song, G. Li, Y. Zhang, B. Rao, S. Xiong and G. He, *Chem. Eng. J.*, 2021, **422**, 130057.

[9] J. Ding, C. Zheng, L. Wang, C. Lu, B. Zhang, Y. Chen, Y. and X. Zhuang, *J. Mater. Chem. A.*, 2019, **7**, 23337-23360.

[10] M. Jiang, Y. Sun, J. Ning, Y. Chen, Y. Wu, Z. Hu, A. Shuja and Meng, *Org. Electron.*, 2020, **83**, 105741.

[11] J. Niu, Y. Wang, X. Zou, Y. Tan, C. Jia, X. Weng and L. Deng, *Appl. Mater. Today*, 2021, **24**, 101073.

[12] X. Lian, Z. Zhao and D. Cheng, *Mol. Cryst. Liq. Cryst.*, 2017, **648**, 223-235.

[13] S. Xiong, J. Wu, M. Chen, K. Zhang, K. Fang, Y. Zhang, X. Wang, C. Hua, C. Jia and B. Wu, *J. Electrochem. Soc.*, 2024, **171**, 075501.

[14] J. Yan, R. Zhang, Y. Yuan and Y. Yuan, *Chinese J. Org. Chem.*, 2019, **39**, 2009-2017.

[15] T. A. Schaub, T. Mekelburg, P. O. Dral, M. Miehlich, F. Hampel, K. Meyer and M. Kivala, *Chem. Eur. J.*, 2020, **26**, 3264-3269.

[16] S. Zhuang, X. Li and J. Liu. *Dyes Pigm.*, 2021, **193**, 109464.

[17] K. W. Kim, J. K. Lee, X. Tang, Y. Lee, J. Yeo, H. C. Moon and S. H. Kim, *Dyes Pigm.*, 2021, **190**, 109321.

[18] P. S. Hariharan, E. M. Mothi, D. Moon and S. P. Anthony, *ACS appl. Mater. interfaces*, 2016, **8**, 33034-33042.

[19] H. Yue, X. Ju, S. Ming, Y. Zhang, J. Zhao, Y. Du and J. Zhang, *Chem. Eng. J.*, 2024, **502**, 157931.

[20] H. Chu, Y. You, J. Liang, Y. Hou and H. Niu, *ACS Appl. Polym. Mater.*, 2024, **6**, 6800-6811.

[21] S. Wang and D. Mo, *Appl. Mater. Today*, 2024, **40**, 102357.

[22] M. R. A. Raj, C. Yao, G. Balakrishnan Muthuperumal, L, Hu, A. Malinge, M. Frémont and W. G. Skene, *ChemPlusChem*, 2025, **90**, e202400667.

[23] W. You, D. Rotili, T. M. Li, C. Kambach, M. Meleshin, M. Schutkowski and C. Steegborn, *Angew. Chem. Int. Ed.*, 2017, **56**, 1007-1011.

[24] A. Karpe, A. Parab, G. Ganesan, P. Walke and A. Chaskar, *J. Photochem. Photobiol. A. Chem.*, 2022, **431**, 114004.

[25] K. M. Divya, D. P. Savitha, G. A. Krishna, T. M. Dhanya and P. V. Mohanan, *J. Photochem. Photobiol. A. Chem.*, 2022, **431**, 114046.

[26] Q. Liu, W. Wang and M. Liu, *Asian J. Org. Chem.*, 2023, **12**, e202300277.

[27] W. Wang, Q. Liu, Y. Chai, K. Zhao, B. Bian and T. Zhang, *J. Mol. Struct.*, 2024, **1306**, 137829.

[28] P. Allan, M. Ostrowska and B. Patel, *Synlett*, 2019, **30**, 2148-2152.

[29] Y. Qu, P. Pander, O. Vybornyi, M. Vasylieva, R. Guillot, F. Miomandre and P. Audebert, *J. Org. Chem.*, 2020, **85**, 3407-3416.

[30] C. Zhou, T. Zhang, S. Zhang, H. Liu, Y. Gao, Q. Su, Q. Wu, W. Li, J. Chen and B. Yang, *Dyes. Pigm.*, 2017, **146**, 558-566.

[31] F. Zhao, J. Kong, W. Zhang, Z. Kuang and M. Zhou, *J Phys. Chem. Lett.*, 2024, **15**, 2885-2892.

[32] W. Li, Y. Pan, R. Xiao, Q. Peng, S. Zhang, D. Ma and Y. Ma, *Adv. Funct. Mater.*, 2014, **24**, 1609-1614.

[33] T. M. Bawazeer, I. Althagafi, M. Morad, A. M. Munshi, A. A. Bayazeed, A. Alharbi and N. El‐Metwaly, *J. Lumin.*, 2021, **36**, 904-913.

[34] S. Chevreux, C. Allain, L. Wilbraham, K. Nakatani, P. Jacques, I. Ciofini and G. Lemercier, *Faraday Discuss.*, 2015, **185**, 285-297.

[35] M. Li and M. Dincă, *Chem. Sci.*, 2014, **5**, 107-111.

[36] J. Liu, X. Ma, Z. Wang, L. Xu, F. Wang, C. He and X. Lu, *ACS Appl. Electron. Mater.*, 2021, **3**, 1489-1495.

[37] J. Wu, T. Hsiang and G. Liou, *J. Mater. Chem. C*, 2018, **6**, 13345-13351.

[38] J. Wu and G. Liou, *Chem. Comm.*, 2018, **54**, 2619-2622.

[39] Q. Tian, J. Xu, Y. Sha, X. Zhu and W. Chu, *Colloids Surf. A: Physicochem. Engin. Aspe.*, 2024, **694**, 134095.

[40] Z. Xing, S. Jia, S. Li, Q. L. Wang, J. D. Zhong, H. Y. Qi, W. B. Sun, Z. H. Jiang, and Z. Chen, *Electrochim. Acta*, 2023, **452**, 142316.

[41] X. Fang, C. Wang, Q. Tian, J. Zhang, Y. Chen, Z. Sun and W. Chu, *Mater. Lett.*, 2023, **333**, 133659.

[42] Y. Liu, C. Wang, X. Fang, J. Zhang, H. Liu, J. Ma and W. Chu, *Dyes Pigm.*, 2021, **193**, 109516.

[43] Y. Guo, F. Zhang and J. Yang, *J. Adv. in Phys. Chem.*, 2013, **2**, 7-14.

[44] H. F. Yu, K. I. Chen, M. H. Yeh and K. C. Ho, *Sol. Energ. Mat. Sol. C.*, 2019, **200**, 110020.

[45] C. Quinton, V. Alain‐Rizzo, C. Dumas‐Verdes, F. Miomandre, G. Clavier and P. Audebert, *Chem. Eur. J.*, 2015, **21**, 2230-2240.

[46] C. Quinton, V. Alain‐Rizzo, C. Dumas‐Verdes, F. Miomandre and P. Audebert, *Electrochim. Acta*, 2013, **110**, 693-701.

[47] C. Quinton, V. Alain‐Rizzo, C. Dumas‐Verdes, G. Clavier, F. Miomandre and P. Audebert, *Eur. J. Org. Chem.*, 2012, 1394-1403.

[48] C. Chang, H. Yueh and C. Chen, *Org. Lett.*, 2011, **13**, 2702-2705.

[49] L. He, J. Tan, C. Liu, S. Wu, Q. L. Zhang, C. Redshaw and X. L. Ni, *ChemistrySelect*, 2022, **7**, e202201155.

[50] K. Sreenath, T. Thomas and K. Gopidas, *Org. Lett.*, 2011, **13**, 1134-1137.

[51] C. Hassenrück and R. Winter, *Inorg. Chem.*, 2017, **56**, 13517-13529.

[52] X. Rong, J. Liu, J. Wu, C. Li, K. Wang, Z. Lu and Y. Huang, *J. Mater. Chem. C*, 2023, **11**, 9640-9648.

[53] L. Mao, M. Zhou, Y. F. Niu, X. L. Zhao and X. Shi, *Org. Chem. Front.*, 2021, **8**, 4678-4684.
[54] M. Zhou, L. Mao, Y. F. Niu, X.L. Zhao, X. Shi and H. B. Yang, *Chinese Chem. Lett.*, 2022, **33**, 1870-1874.
[55] T. Lu and F. Chen, *J. Comput. Chem.*, 2012, **33**, 580-592.

Data availability

All data included in this study are available upon request by contact with the corresponding author